

LA-UR-20-28902

Approved for public release; distribution is unlimited.

Title: Rossi Alpha Measurements – Rapid Organic (n, gamma) Discrimination
Detector (RAM-RODD) system capabilities

Author(s): Weldon, Robert Allen Jr.
Cutler, Theresa Elizabeth
Hutchinson, Jesson D.
McKenzie, George Espy IV
Misurek, Lauren Ashley
Sorensen, Eric Byron

Intended for: Report

Issued: 2021-07-09 (rev.1)

Disclaimer:

Los Alamos National Laboratory, an affirmative action/equal opportunity employer, is operated by Triad National Security, LLC for the National Nuclear Security Administration of U.S. Department of Energy under contract 89233218CNA000001. By approving this article, the publisher recognizes that the U.S. Government retains nonexclusive, royalty-free license to publish or reproduce the published form of this contribution, or to allow others to do so, for U.S. Government purposes. Los Alamos National Laboratory requests that the publisher identify this article as work performed under the auspices of the U.S. Department of Energy. Los Alamos National Laboratory strongly supports academic freedom and a researcher's right to publish; as an institution, however, the Laboratory does not endorse the viewpoint of a publication or guarantee its technical correctness.

Rossi Alpha Measurements – Rapid Organic (n, γ) Discrimination Detector (RAM-RODD) system capabilities

Robert Allen Weldon Jr.,* Theresa Elizabeth Cutler,* Jesson D. Hutchinson,*
Geordie Espy McKenzie IV,* Lauren Misurek*, Eric Byron Sorensen*

Abstract

The Rossi Alpha Measurements–Rapid Organic (n, γ) Discrimination Detector (RAM-RODD) is an array organic scintillation detectors that has been optimized for use in neutron noise measurements. This report details the capability of the system including the method of energy calibration, pulse shape discrimination, and time resolution.

I. INTRODUCTION

RAM-RODD is an organic scintillator based measurement system composed of eight 5.08 cm (\varnothing) \times 5.08 cm EJ-309 liquid scintillators. Organic scintillators offer significantly faster timing resolution compared to commonly used ^3He based detector systems (e.g. the MC-15 [1]) due to the method of neutron detection. ^3He based systems often rely on moderating fast neutrons to lower energies for increased detection efficiency of the $^3\text{He}(n,p)^3\text{H}$ reaction and have time resolutions on the order of hundreds of ns to μs . In contrast, organic scintillators directly detect fast particles via elastic scatter with time resolutions on the order of hundreds of ps to ns. The excellent time resolution makes organic scintillators well suited for measurements that employ time-correlated neutron noise analysis techniques such as Feynman-alpha analysis [2] and Rossi-alpha analysis [3]. RAM-RODD is based on OSCAR, a stilbene based organic scintillator measurement system which has shown very promising results for time-correlated neutron noise measurements [4]–[6].

RAM-RODD has been optimized for neutron noise measurements of special nuclear material (SNM) such as highly enriched uranium (HEU) and weapons grade plutonium. The system will be leveraged in future measurements at the National Criticality Experiments Research Center (NCERC) including IER-488 Measurements of Uranium Subcritical and Critical (MUSiC) [7]. This report summarizes the selection and optimization of several system settings including (1) high voltage, (2) calibration, (3) pulse shape discrimination, and (4) time resolution.

II. EQUIPMENT

The system consists of (1) eight 5.08 cm (\varnothing) \times 5.08 cm EJ-309 liquid scintillators, (2) an eight channel CAEN R1470ETD desktop power supply module, (3) an eight channel CAEN DT5730 (500 MHz, 14 bit) digitizer, and (4) a data acquisition computer. Drawings of the detector model provided by the manufacturer are shown in Figures 1a and 1b. Figure 1a shows the photomultiplier tube (PMT) and base components. The PMT is a 51 mm diameter Hamamatsu R7724 [8]. Figure 1b shows the assembled detector and the aluminum housing. Data acquisition is performed using CAEN's CoMPASS software [9].

Data can be acquired using the 5730 digitizer and CoMPASS either as full waveforms or using the digital pulse processing (DPP) firmware available via field-programmable gate arrays (FPGAs) included in the digitizer. The

*Nuclear Engineering and Nonproliferation 2, Los Alamos National Laboratory, P.O. Box 1663, Los Alamos, NM, 87545, raw@lanl.gov

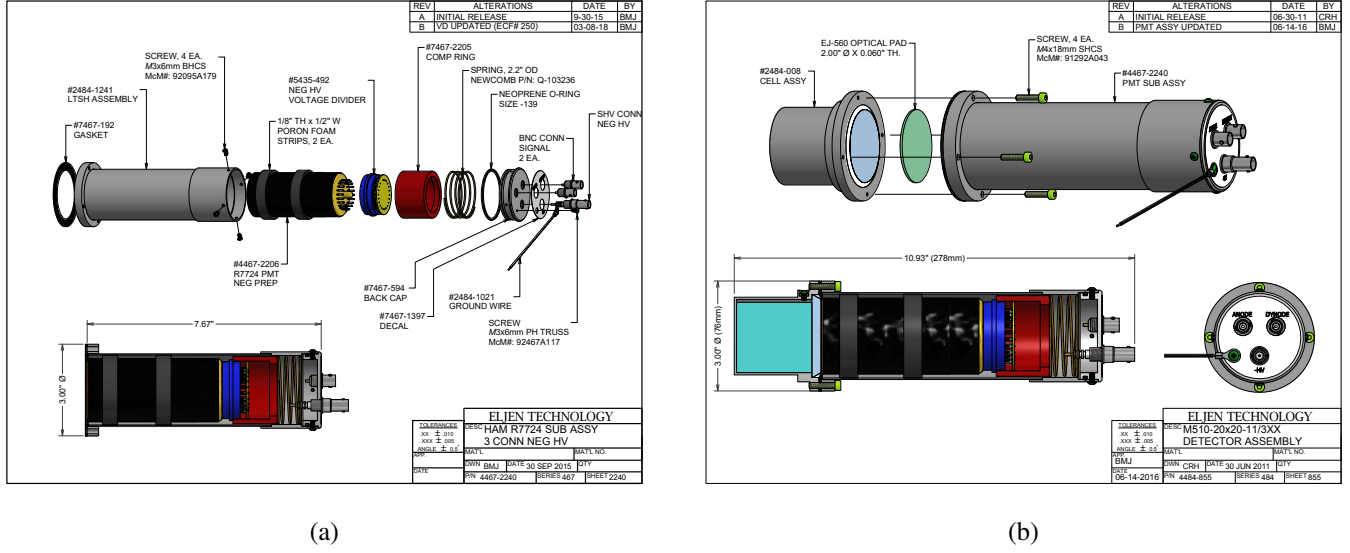


Fig. 1: Drawings of PMT with housing (a) and complete detector (b).

DPP firmware is particularly suited for high count rate measurements because it reduces the data throughput from the number of points composing a waveform (generally >100 for applications such as neutron noise measurements) to 3. The 3 quantities analyzed using the DPP firmware are (1) the full wave form integrated charge (Q_l), (2) a short gate integrated charge (Q_s), and (3) the trigger time. Q_l relates to the energy deposited (refer to [10] for a detailed description and for the relationship between Q_l and the neutron energy deposition for EJ-309). The ratio of Q_s to Q_l is used to perform pulse shape discrimination and is discussed in Section V.

III. HIGH VOLTAGE

The high voltage (HV) settings were selected based on the following criteria: (1) the dynamic range of the CAEN 5730 digitizer, (2) the majority of neutron interactions in the scintillator will deposit <10 MeV, and (3) obtaining a time resolution <1 ns. The digitizer has two dynamic ranges — 0.5 V and 2 V. The 0.5 V dynamic range was selected to optimize the system resolution (time and energy). The system is designed primarily for measurements of SNM, therefore, the maximum neutron energy deposition anticipated is ~ 10 MeV. Note that higher energy neutrons are created in fission but they are (1) rare and (2) unlikely to deposit their full energy in a single elastic scatter. The majority of the detected neutrons are expected to deposit between 0.5 and 6 MeV.

The HV was set to reduce the resolution of the most probable neutron energy depositions while also including most of the desired energy range without saturating the digitizer. This was achieved by setting HV such that the maximum pulse integral corresponded to neutron energy depositions of ~ 7 MeV. This selection provides good resolution over the primary energy range of interest (0.5 – 6 MeV) while also including most of the higher energy interactions. Note that, while the maximum pulse integral corresponds to ~ 7 MeV, the system can still measure higher energy interactions, but the pulse integral will no longer have the same relationship with the energy deposition. This effect is known as saturating the digitizer. Energy information is lost for saturated pulses, but the timing is essentially unaffected. In short, the settings reported here are appropriate for neutron noise measurements that only rely on the trigger time, but they are only appropriate for applications where the energy of the interaction is needed, such as neutron spectroscopy, if depositions >7 MeV are discarded.

The selected voltages for each detector are shown in Table I. Note that the HV settings for each detector were selected individually and are unique values. This is generally necessary, even for detectors with identical PMT

types, due to inherent differences in the bias requirements of the dynode chains among other factors. The nominal voltage is 1000 V. The impact of these settings on the time resolution will be discussed in Section VI.

TABLE I: Detector voltages for neutron noise measurements with RAM-RODD. The detector number (Detector) corresponds to the last digit of the EJ-309 detector serial numbers.

Detector	1	2	3	4	5	6	7	8
Voltage (V)	978	1036	1023	1058	1043	962	1088	964

IV. DETECTOR ENERGY CALIBRATION

The detectors are calibrated using a method similar to that proposed by Dietze [11], [12]. Calibrations are performed relative to the ^{137}Cs 662 keV γ Compton edge (477 keV). A ^{137}Cs source is placed at a fixed distance from the detector, and the energy spectrum is measured. Note that the source should be placed far enough from the detector such that the emitted gammas enter the detector normal to the detector face (i.e. as a planar source) when possible. The measured, background-subtracted spectrum is truncated to the vicinity of the Compton edge, and a least squares minimization is performed to fit a simulated spectrum to the measured spectrum.

The simulated spectra is obtained using a Monte Carlo code (MCNPX-PoliMi [13] was used for the results presented here). The simulation should include the γ source distribution and the scintillator material. The scintillator housing can also be modeled, but the spectrum is generally not significantly affected by its inclusion. The simulated data is folded with the resolution function

$$\sigma_L = \alpha Q_l \quad (1)$$

where α is the resolution parameter and Q_l is the integrated charge. The amplitude of the simulated spectrum is scaled to the measured spectrum using a power law

$$y = a Q_l^k \quad (2)$$

where y is the spectrum amplitude in counts and a, k are fit parameters. Scaling with Equation 2 is a modification to Dietze's method that removes the need to precisely simulate electron transport in the scintillator and surrounding materials [14]. The scaling, resolution, and channel number corresponding to the edge location are determined by simultaneously fitting the simulated spectrum to the truncated measured spectrum.

An example of the measured spectrum and fitted simulated spectrum is shown in Figure 2a. The measured and simulated spectra are truncated to the plotted region for the fit (0.3 – 0.6 MeV). The residuals of the fit are shown in Figure 2b and show that the data is well reproduced by the fit. The light output is defined relative to the 477 keV ^{137}Cs Compton edge location. Note that this definition of relative light yield does not make the assumption of linearity in the electron light yield which has traditionally been made in the literature. Recent work has drawn the assumption of electron light yield linearity into question for many commonly used organic scintillators [15]. The issue is avoided by the simplistic formulation of the scintillator light output implemented here.

V. PULSE SHAPE DISCRIMINATION

The relative magnitudes of the tails of scintillation pulses are known to have a dependence on the type of exciting particle for some organic scintillators [16]. This dependence can be used to distinguish between different

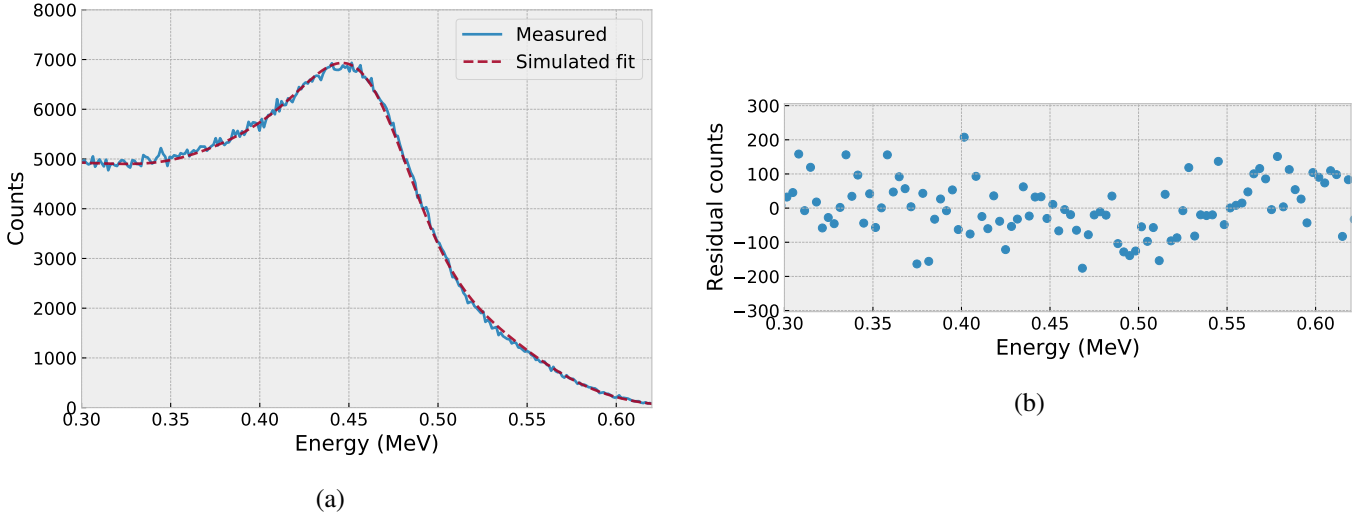


Fig. 2: (a) ^{137}Cs measured and fitted simulated spectra. (b) Fit residual counts.

types of incident radiation via pulse shape discrimination (PSD). PSD can be implemented in many ways, but the most common method (and the method implemented in this work) is performed by taking the ratio of the charge integrated over a truncated portion of the pulse (called the short gate integral or Q_s) to the charge integrated over the full pulse (called the long gate integral or Q_l).

PSD is implemented in RAM-RODD using the DPP firmware by having it calculate a short gate integral at the start of the pulse and a long gate integral. The ratio Q_s/Q_l is called the pulse shape parameter. An example of PSD is shown in Figure 3a. The length of the long gate is determined by the length of the scintillation pulses. For EJ-309, 95% of the scintillation light is detected within 300 ns of the beginning of the pulse, so a 300 ns gate was selected for the long gate. The short gate length is selected by optimizing the figure of merit (FOM) of the PSD.

The FOM is commonly defined as

$$\text{FOM} = \frac{|\mu_\gamma - \mu_n|}{\text{FWHM}_\gamma + \text{FWHM}_n} \quad (3)$$

where μ_γ is the centroid of the γ peak, μ_n is the centroid of the neutron peak, and FWHM is the full width at half maximum. The FOM is simply a unitless value defining the separation between the different particles (in this case γ and neutron) in terms of the pulse shape parameter. A single value can be obtained for the FOM by projecting the pulse shape parameter onto the pulse shape parameter axis and fitting the two bands with a double Gaussian. A problem with this method is that there is generally some curvature to the pulse shape parameter versus Q_l as seen in Figure 3a. The FOM will therefore not be representative of the true separation between the bands which has a dependence on Q_l .

To address this the FOM is calculated for energy cuts of the pulse shape parameter in Q_l as shown by the black lines in Figure 3a. Figure 3b shows the data between the black lines in Figure 3a projected onto the PSD parameter axis and fit with a double Gaussian. This same process is repeated over the entire Q_l range, and the FOM dependence on Q_l can be plotted as in Figure 4. Note that the x-axis in Figure 4, labeled “Light output,” is Q_l relative to Q_l of a 477 keV electron as discussed in Section IV.

VI. TIME RESOLUTION

The CAEN 5730 digitizer has two onboard options for determining the time stamp corresponding with the beginning of a pulse — leading edge discrimination (LED) and constant fraction discrimination (CFD). A fixed

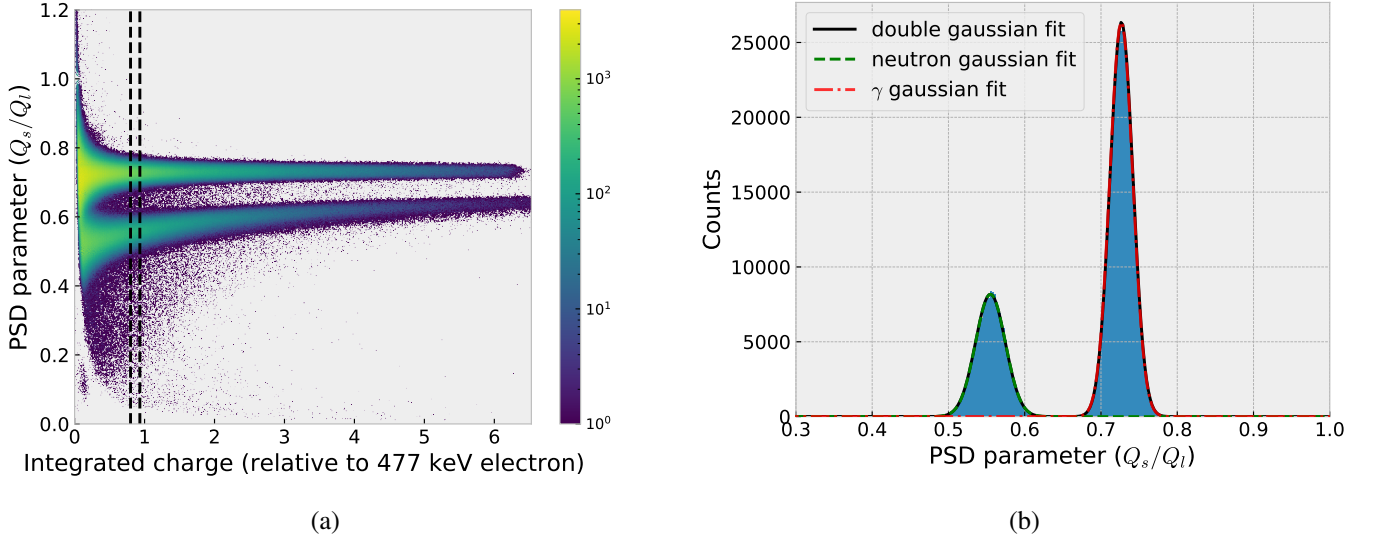


Fig. 3: PSD parameter versus integrated charge (a), and double Gaussian fit to the γ and neutron bands (b). The bottom band in (a) corresponds to neutron interactions and the top band to γ interactions. The data between the black lines in (a) is the same data that is fit with the double Gaussian in (b).

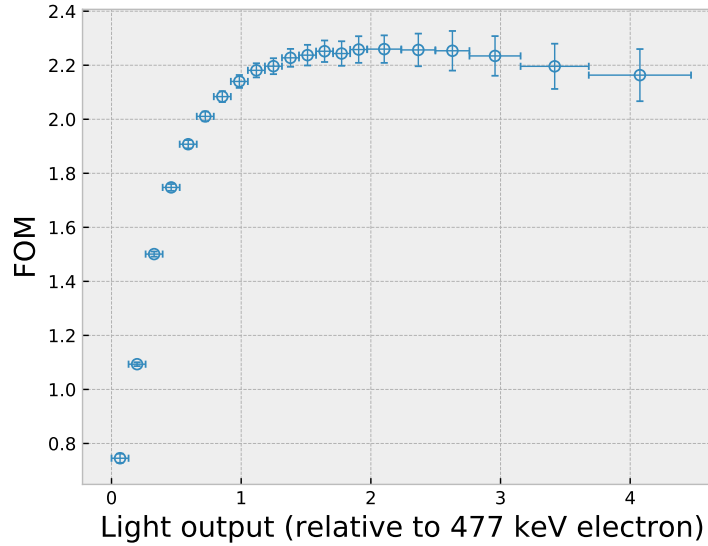


Fig. 4: The FOM dependence on the integrated charge (or light output) relative to a 477 keV electron's integrated charge.

threshold is set with the LED method, and the time stamp when a pulse crosses the threshold is used as the trigger time. While the LED method is simple to implement, it suffers from issues such as amplitude walk, where the trigger time has a dependence on the pulse amplitude. These issues are avoided by using CFD which does not rely on the amplitude of the pulse.

CFD was originally an analog technique which can be implemented digitally using the same concepts with an FPGA. The pulse is attenuated by an attenuation factor which is equal to some constant fraction of the pulse amplitude (in analog systems this was generally selected to cover between 10% – 90% or 20% – 80% of the pulse rise time). The original signal is also inverted and delayed by a time greater than the pulse rise time. The attenuated

and delayed-inverted signals are summed to produce a bipolar pulse. The zero crossing of the bipolar pulse is taken as the trigger time.

The time resolution of the system is optimized by selecting the CFD parameters that minimize the spread in the trigger time. One method of performing this optimization is to use a γ source that emits photons simultaneously at 180° relative to each other. The source is placed between of the detectors and coincident hits in the detectors are recorded. Note that for the results reported here a ^{22}Na source was “sandwiched” between the detectors. The difference in time between the coincident counts in the two detectors is calculated and histogrammed as shown in Figure 5a. The histogram is fit with a Gaussian and the FWHM is calculated. The FWHM value is the time resolution. Note that the offset in the time difference in Figure 5a is due to differences between the transit time spreads of the two detectors. This effect does not need to be corrected because it is a constant offset and does not influence the width of the peak.

The optimized parameter values were determined by performing measurement with combinations of attenuation factors and delays. The 5730 digitizer firmware offers delays in 2 ns increments (the 5730 has a 500 MHz sampling which corresponds to a sample every 2 ns) and attenuation factors of 25%, 50%, 75%, and 100%. The results of the measurements are shown in Figure 5b. The optimized parameters are a delay of 10 ns and an attenuation factor of 25% resulting in a time resolution of 0.90 ns.

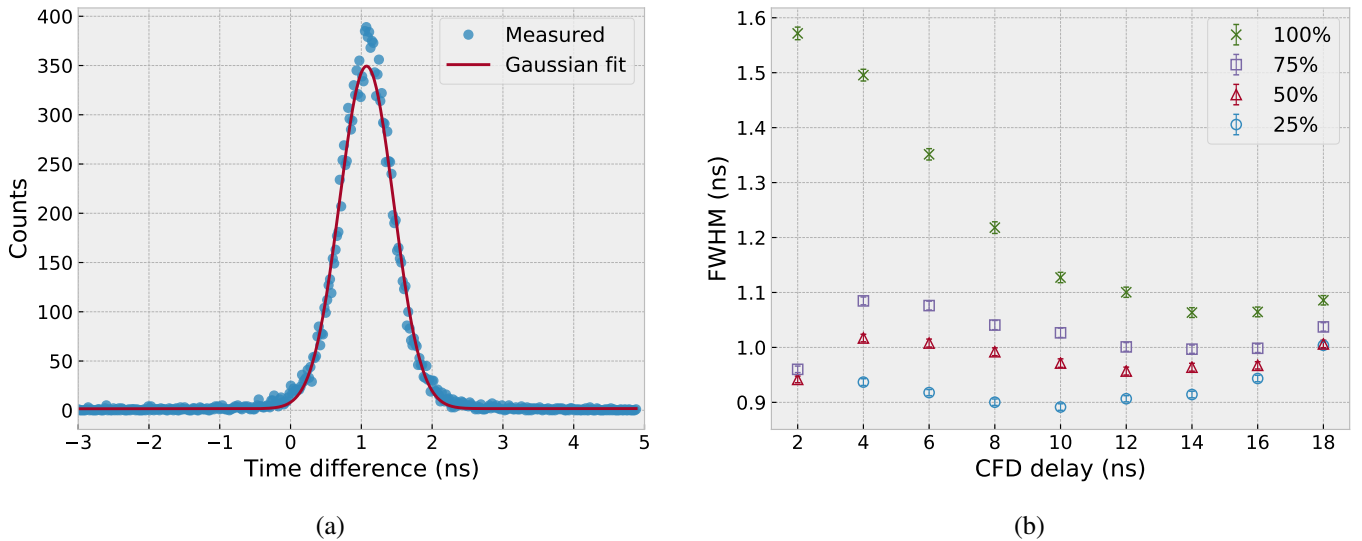


Fig. 5: (a) Difference in the arrival time of annihilation photons from a ^{22}Na γ source measured by two EJ-309 detectors. (b) CFD optimization results. The FWHM is plotted against the CFD delay for each attenuation factor (legend).

Several points should be noted regarding the “optimized” time resolution. (1) Better timing resolution is achievable when analyzing full waveforms and implementing an offline CFD algorithm rather than relying on the digitizer’s DPP firmware. (2) The time resolution has a dependence on the HV. This was not explored in this work because the HV was specifically set to detect neutron interaction up to 7 MeV. Increasing the HV would result in a better time resolution, but it would also result in a loss of the relationship between Q_l and energy deposition for lower energy neutron interactions. (3) The time resolution was calculated using only two of the eight detectors. It is considered to be accurate for all of the detectors because they are identical.

VII. CONCLUSION

An organic scintillator array designed for use in neutron noise measurements has been optimized. The energy calibration and pulse shape discrimination abilities were discussed. The HV was set to maintain an accurate relationship between the light output and the neutron energy depositions up to ~ 7 MeV. The digitizer's onboard CFD timing capability was optimized for the system, and a time resolution of 0.9 ns was obtained.

ACKNOWLEDGMENT

This work was supported by the DOE Nuclear Criticality Safety Program, funded and managed by the National Nuclear Security Administration for the Department of Energy.

REFERENCES

- [1] C. E. Moss, E. B. Sorensen, and M. A. Smith-Nelson, *MC-15 user manual*, Los Alamos National Laboratory, LA-UR-16-27099, 2016.
- [2] R. P. Feynman, F. De Hoffmann, and R. Serber, "Dispersion of the neutron emission in u-235 fission," *Journal of Nuclear Energy (1954)*, vol. 3, no. 1-2, pp. 64–IN10, 1956.
- [3] J. D. Orndoff, "Prompt neutron periods of metal critical assemblies," *Nuclear Science and Engineering*, vol. 2, no. 4, pp. 450–460, 1957.
- [4] M. Y. Hua, C. A. Bravo, A. T. MacDonald, J. D. Hutchinson, G. E. McKenzie, B. C. Kiedrowski, S. D. Clarke, and S. A. Pozzi, "Rossi-alpha measurements of fast plutonium metal assemblies using organic scintillators," *Nuclear Instruments and Methods in Physics Research Section A: Accelerators, Spectrometers, Detectors and Associated Equipment*, vol. 959, p. 163507, 2020.
- [5] M. Y. Hua, J. D. Hutchinson, G. E. McKenzie, B. C. Kiedrowski, M. W. Liemohn, S. D. Clarke, and S. A. Pozzi, "Measurement uncertainty of Rossi-alpha neutron experiments," *Annals of Nuclear Energy*, vol. 147, p. 107672, 2020.
- [6] M. Y. Hua, F. B. Darby, J. D. Hutchinson, G. E. McKenzie, S. D. Clarke, and S. A. Pozzi, "Validation of the two-region Rossi-alpha model for reflected assemblies," *Nuclear Instruments and Methods in Physics Research Section A: Accelerators, Spectrometers, Detectors and Associated Equipment*, vol. 981, p. 164535, 2020.
- [7] R. Weldon, T. E. Cutler, J. D. Hutchinson, W. L. Myers, G. E. McKenzie IV, A. T. McSpaden, and R. G. Sanchez, "Application of the rossi-alpha method to simulations of heu and organic scintillators," 2020, to be published in: *Proceedings of The American Nuclear Society (2020 ANS Winter Meeting)*.
- [8] <https://www.hamamatsu.com/us/en/product/type/R7724/index.html>, Accessed: 10/19/2020.
- [9] <https://www.caen.it/products/compass/>, Accessed: 10/19/2020.
- [10] J. Brown, B. L. Goldblum, T. Laplace, K. Harrig, L. Bernstein, D. Bleuel, W. Younes, D. Reyna, E. Brubaker, and P. Marleau, "Proton light yield in organic scintillators using a double time-of-flight technique," *Journal of Applied Physics*, vol. 124, no. 4, p. 045101, 2018.
- [11] G. Dietze, "Energy calibration of NE-213 scintillation counters by δ -rays," *IEEE Transactions on Nuclear Science*, vol. 26, no. 1, pp. 398–402, 1979.
- [12] G. Dietze and H. Klein, "Gamma-calibration of NE 213 scintillation counters," *Nuclear Instruments and Methods in Physics Research*, vol. 193, no. 3, pp. 549–556, 1982.
- [13] S. A. Pozzi, E. Padovani, and M. Marseguerra, "Mcnp-polimi: a monte-carlo code for correlation measurements," *Nuclear Instruments and Methods in Physics Research Section A: Accelerators, Spectrometers, Detectors and Associated Equipment*, vol. 513, no. 3, pp. 550–558, 2003.
- [14] R. Weldon, J. Mueller, C. Awe, P. Barbeau, S. Hedges, L. Li, M. Mishra, and J. Mattingly, "Characterization of stilbene's scintillation anisotropy for recoil protons between 0.56 and 10 MeV," *Nuclear Instruments and Methods in Physics Research A*, vol. 977, pp. 164–178, 2020.
- [15] S. A. Payne, W. W. Moses, S. Sheets, L. Ahle, N. J. Cherepy, B. Sturm, S. Dazeley, G. Bizarri, and W.-S. Choong, "Nonproportionality of scintillator detectors: Theory and experiment. II," *IEEE Transactions on Nuclear Science*, vol. 58, no. 6, pp. 3392–3402, 2011.
- [16] L. M. Bollinger and G. E. Thomas, "Measurement of the time dependence of scintillation intensity by a delayed-coincidence method," *Review of Scientific Instruments*, vol. 32, no. 9, pp. 1044–1050, 1961.